Introduction to High-Efficiency Klystrons

1. Abstract

The klystron, which provides RF power to large-scale particle accelerators, is one of the most power-consuming devices. Therefore, high-efficiency klystrons are in strong demand. Previous OHO lectures [1][2][3] have detailed the theories and technologies of the klystron. This lecture will primarily focus on the efficiency of a klystron, discussing the ballistic theory of the klystron RF section. Through these discussions, we will define efficiency and highlight concepts critical to high-efficiency klystron design. Code for plotting Applegate diagrams based on equations will be provided. Additionally, simulation tools for designing klystrons will be introduced. Various new bunching methods aimed at achieving higher klystron efficiency will be described in detail, with some examples of input data for a one-dimensional simulation tool to help intuitively understand these new technologies. The advantage of multi-beam klystrons in achieving high efficiency will also be discussed. In the final part of the lecture, parameters of existing high-efficiency klystrons will be listed in detail. Ongoing global research activities, including new designs and test results, will be introduced individually.

2. Introduction

2.1. RF power of a klystron

Klystron, initially developed in the 1930s [4] is an amplifier of microwave power. Owing to its high gain, efficiency, and ease of handling and maintenance, klystrons are widely adopted by particle accelerators as RF power sources.

Driven by decades of evolving requirements from particle accelerators, klystrons for scientific use have seen significant advancements in both pulsed output power and average output power. Table 1 lists examples of klystrons with their output power levels [5][6][7][8]. Pulsed klystrons, typically used in linear accelerators, are required in quantities of tens or even hundreds. Consequently, these klystrons are among the most power-consuming components in linear accelerators. Similarly, UHF band continuous-wave (CW) klystrons, with average RF power reaching megawatt levels, are significant power-consuming devices.

Table 1 Examples of klystrons for accelerators with their output power levels

Vendor	**CANON**	**SLAC**	**SLAC**	**CANON**
Peak power (MW)	50	65	150	1.2
Average power (MW)	0.01	0.041	0.027	1.2
Frequency (GHz)	2.856	2.856	2.998	0.509
Operation mode	Pulsed	Pulsed	Pulsed	CW
Type	E3730A	5045		E3786

2.2. RF power consumption by large-scale accelerators

The KEK e^-/e^+ Injector Linac operates with 60 pulsed 50 MW S-band klystrons [5]. The efficiency of those 50 MW klystrons is 45%. The power consumed solely by these klystrons is 1.23 MW, not accounting for the electrical transformation efficiency of the modulators and the power consumption by the focusing magnets [9]. If the klystron efficiency could be improved from 45% to 65%, a total power of 0.38 MW would be saved. Over an entire year of operation, this would result in an energy savings of 2,270 MWh. To achieve this, an 80 MW multi-beam klystron (MBK) with an enhanced efficiency of up to 70% is under development to replace the existing 50 MW klystrons.

The RF sources for the rings of SuperKEKB utilize 32 CW 1.2 MW UHF-band klystrons [8] ,but they operate at the 400-kW level. The state-of-the-art efficiency of these UHF-band klystrons is 65%, resulting in a total power consumption of 20 MW. If the efficiency of the UHF-band klystrons could be improved from 65% to 80%, a significant power saving of 3.7 MW would be achieved. This saved power would cover the total power consumption of the KEK e^-/e^+ Injector Linac.

Table 2 RF power consumptions by large-scale accelerators

Project name	RF power consumption
KEK e^-/e^+ Injector Linac	1.23 MW
Rings of SuperKEKB	20 MW
ILC	54 MW
FCC	160 MW
CLIC	118 MW
CEPC	174 MW

Proposed by the Japanese high-energy physics community, the International Linear Collider (ILC) will require the L-band MBK to generate a total of 35 MW of RF power for accelerating electrons and positrons to super-high energies [10]. With the state-of-the-art efficiency of the MBK at 65%, a significant amount of electric power will be wasted by the RF source itself. The efficiency of klystrons has become a worldwide topic, as power consumption is a common challenge for future large-scale accelerators, such as the FCC [11], CLIC [12], and CEPC [13]. In Table 2, we list the RF power consumption for some of the existing and future large-scale accelerators. The amount of power consumption for these future projects is astonishing. The proposed large-scale accelerators increasingly demand high-efficiency klystrons to reduce massive operating costs.

3. Basics of the RF section

3.1. Structure of a klystron

As shown in Fig. 1, a klystron is composed of an electron gun region, an interaction region, and a collector region. The electron gun primarily includes the cathode, filament,

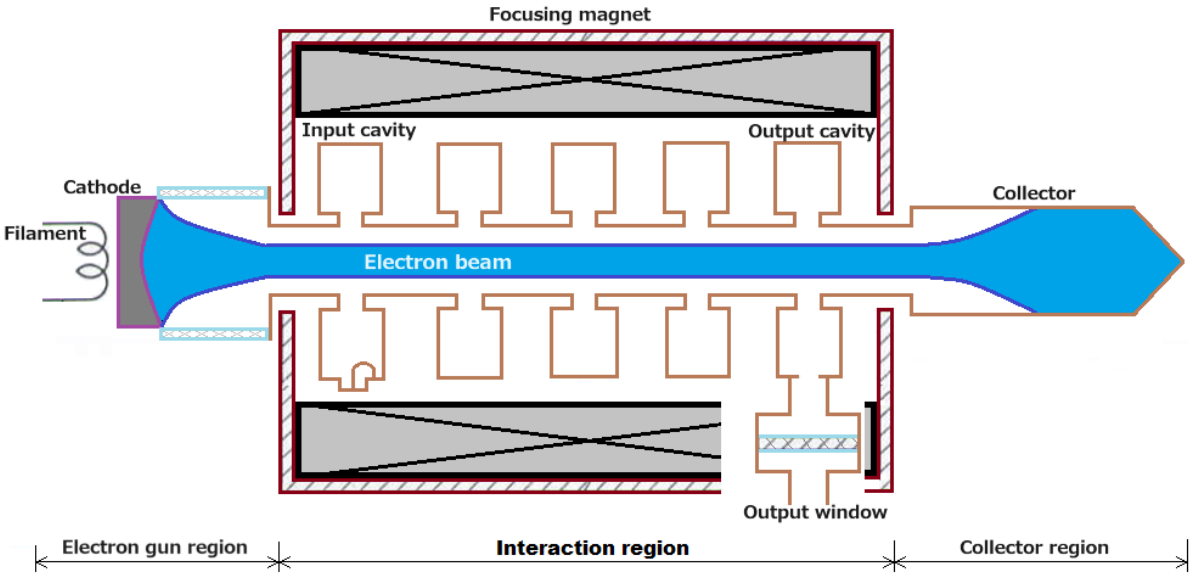

Fig. 1 The structure of a klystron

insulating ceramic, and other components. The filament heats up the cathode, allowing electrons to escape from its surface. A high voltage is applied across the ceramic cylinder, accelerating the electrons from the cathode to the anode. As a result, the electrons gain energy and form an electron beam with a specific energy level. The basic parameters that describe the electron beam are its current and voltage (which is the same as the gun voltage).

The electron beam drifts through the tunnel and cavities located in the interaction region. As the beam passes through the input (first) cavity, it encounters the RF voltage across the gap, causing some electrons to accelerate and others to decelerate depending on the phase of the voltage. This process is known as velocity modulation. This velocity modulation causes density modulation through the drift tunnel, forming electron bunches. These bunches induce RF in successive cavities, producing gap voltages. The velocity modulation is then reinforced, and density modulation is strengthened. Finally, the well-bunched beam induces a substantial RF power at the output (last) cavity and decelerates. The RF power flows through the output window to a microwave transmission line. The decelerated electrons, or spent beam, drift into the collector region, where a cooled collector stops the spent beam.

The electron beam serves as the power-amplifying medium. It gains power in the gun region, forms bunches, transfers part of its power to microwaves in the interaction region, and finally stops, losing the rest of its power in the collector region. In simple terms, a high-efficiency klystron transfers more power in the interaction region rather than losing it in the collector region.

Due to the Coulomb force among electrons, the beam formed by many electrons exhibits space charge force. Transversely, this results in the expansion of the beam, necessitating a focusing magnet to prevent it from spreading. Longitudinally, the space charge force causes an anti-bunching effect, complicating the processes of velocity and density modulation. More details will be discussed in Section 3.2.4.

3.2. Velocity modulation

3.2.1. The basic analysis

The principle of the electron bunching process in a klystron is based on the modulation of electron velocity [14]. A few assumptions are introduced first for the convenience of explaining the velocity modulation.

1) The length of modulation gap (or cavity gap) is zero.
2) The modulation voltage (or the voltage across the first cavity gap) is considered negligibly small compared to the DC beam voltage. This is usually referred to as a "small signal".
3) The space charge force is not considered.
4) The velocity of the electrons is much slower than the speed of light, which means relativistic effects are neglected.

A sine wave voltage is applied across the first cavity gap.

$$V_1 = \hat{V}_1 \sin \omega t \quad (1)$$

Where V_1 represents the time-varying voltage across the cavity gap, $\hat{V}_1$ is the magnitude of the modulation voltage, t is the time and ω is the angular frequency of sine wave voltage applied to the modulation gap.

Before passing through the modulation gap, the DC beam voltage can be

$$V_0 = \frac{1}{2}\frac{m}{e}v_0^2 \quad (2)$$

Where m and e are the mass and electric charge of an electron, respectively. V_0 is the DC

beam voltage. v_0 is the velocity of an electron with the DC beam voltage.

Once an electron passes through the modulation gap at the time t_1, its velocity is modified by the gap voltage. According to the law of conservation of energy, the following relationship can be expressed

$$\frac{1}{2}mv^2 = e\left(V_0 + \hat{V}_1 \sin \omega t_1\right) \qquad (3)$$

Where v is the modified velocity of the electron.

Combine the Eq. (2) and Eq. (3), then

$$v = v_0\left(1 + \frac{\hat{V}_1}{V_0}\sin \omega t_1\right)^{\frac{1}{2}}$$

$$= v_0\left(1 + \frac{1}{2}\frac{\hat{V}_1}{V_0}\sin \omega t_1 - \frac{1}{8}\left(\frac{\hat{V}_1}{V_0}\right)^2 \sin^2 \omega t_1 + \cdots\right) (4)$$

Owing to assumption 2), the $\hat{V}_1/V_0$ is a small value. By neglecting second-order and higher-order terms, the relationship can be simplified to

$$v = v_0\left(1 + \frac{1}{2}\frac{\hat{V}_1}{V_0}\sin \omega t_1\right) \qquad (5)$$

Equation (5) indicates that a sine wave gap voltage results in a sine wave velocity modulation of the electron, given assumption 2).

If the electron enters the modulation gap at t_1 and drifts a length l downstream of the modulation gap by time t_2. Using Eq. (4) and then t_2 can be expressed as follows

$$t_2 = t_1 + \frac{l}{v_0\left(1 + \frac{\hat{V}_1}{V_0}\sin \omega t_1\right)^{\frac{1}{2}}}$$

$$= t_1 + \frac{l}{v_0}\left(1 - \frac{1}{2}\frac{\hat{V}_1}{V_0}\sin \omega t_1 + \frac{3}{8}\left(\frac{\hat{V}_1}{V_0}\right)^2 \sin^2 \omega t_1 + \cdots\right) (6)$$

Again, neglecting the second order and higher order terms, t_2 can be expressed as follows

$$t_2 = t_1 + \frac{l}{v_0}\left(1 - \frac{1}{2}\frac{\hat{V}_1}{V_0}\sin \omega t_1\right) \qquad (7)$$

It follows that

$$\omega t_2 = \omega t_1 + \theta_0 - X \sin \omega t_1 \qquad (8a)$$

$$\left\{\begin{array}{c} \theta_0 = \dfrac{\omega l}{v_0} \\ X = \dfrac{1}{2}\alpha\theta_0 \\ \alpha = \dfrac{\hat{V}_1}{V_0} \end{array}\right\} \qquad (8b)$$

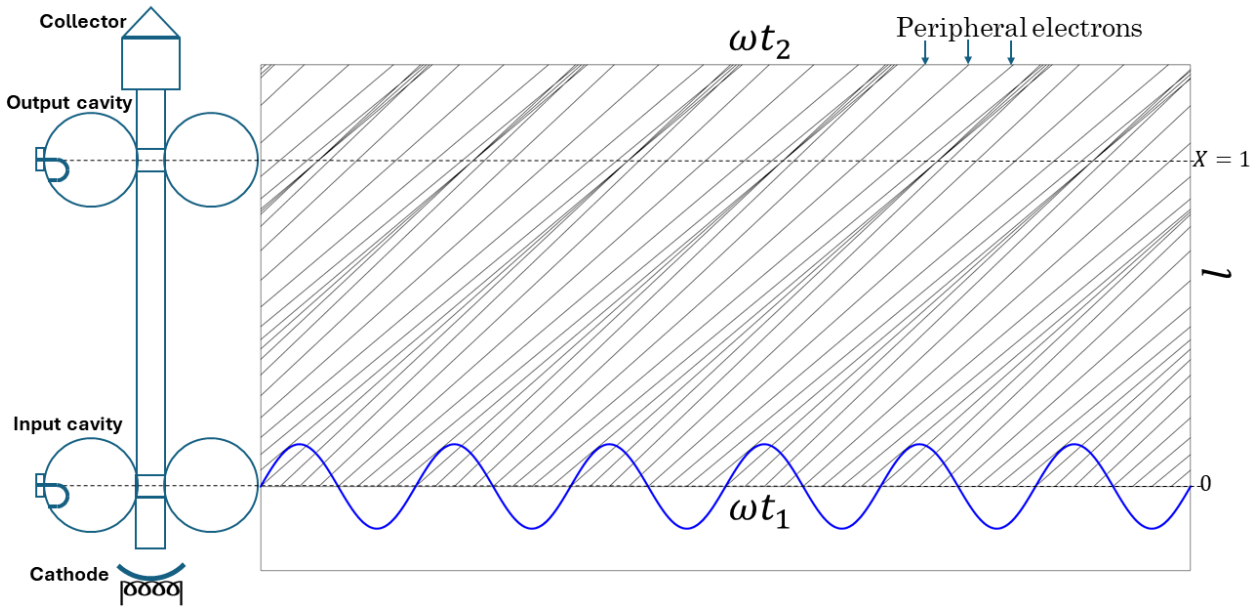

Fig. 2 The Applegate diagram of a two-cavity klystron

(The code for plotting is listed in Appendix 1)

The θ_0 is called the DC transit angle of the electron reaching the distance of l. The X is called the bunching parameter. The α is a depth of modulation. In assumption 2), the α is considered to be a small number.

From Eq. (8a), we can draw the well-known Applegate diagram, as shown in Fig. 2. It illustrates that electrons with a DC beam velocity enter the modulation gap of the input cavity, resulting in the electrons arriving at the output cavity in bunches. The MATLAB [15] code for generating the plot shown in Fig. 2, which is based on Eq. (8a), is provided in Appendix 1.

In Fig. 2, the output cavity is positioned where electrons begin to "meet" each other, at $X = 1$. Once the $X > 1$, ωt_1 becomes a multivalued function of ωt_2, indicating that the electrons have overtaken each other. In fact, to achieve maximum electron efficiency in the two-cavity klystron, the output cavity should be positioned further downstream. This will be discussed in Section 3.2.2.

3.2.2. The electron efficiency

The Eq. (8a) can be matched to Kepler's equation if ωt_1 is considered as the independent variable and $(\omega t_2 - \theta_0)$ is treated as the dependent variable

$$(\omega t_2 - \theta_0) = \omega t_1 - X \sin \omega t_1 \quad (9)$$

Then the ωt_1, as a solution to Kepler's equation, can be written directly as

$$\omega t_1 = (\omega t_2 - \theta_0) + \sum_{n=1}^{\infty} \frac{2}{n} J_n(nX) \sin n(\omega t_2 - \theta_0) \quad (10)$$

Where J_n is the Bessel function of the nth order. The current components I_2 in the beam can be calculated by (Based on the Law of Conservation of Charge: $I_2 * |dt_2| = I_0 * |dt_1|$)

$$I_2 = I_0 \frac{dt_1}{dt_2} \quad (11)$$

Where I_0 is the DC beam current. With applying Eq. (10) into Eq. (11), the current components I_2 can be expressed as

$$I_2 = I_0(1 + \sum_{n=1}^{\infty} i_n) \quad (12a)$$

$$i_n = 2J_n(nX) \cos n(\omega t_2 - \theta_0) \quad (12b)$$

Where i_n represents the nth order AC current component in the beam.

According to the characteristic of the Bessel function, once $X = 1.84$, J_1 reaches its maximum value of $J_1(1.84) = 0.58$. Therefore, the maximum value of the fundamental component of the current will be $i_{1,MAX} = 1.16 I_0$.

The output RF power of the klystron is

$$P_{out} = \frac{1}{2} \hat{V}_2 i_1 \quad (13)$$

Where the $\hat{V}_2$ is the magnitude of the gap voltage of output cavity. If $\hat{V}_2 = V_0$ (to ensure the electrons are decelerated to the maximum extent without any electrons being reversely accelerated), then the theoretical maximum electron efficiency of a two-cavity klystron is

$$\eta = \frac{P_{out}}{P_0} = \frac{1}{2} \frac{i_{1MAX}}{I_0} = 58\% \quad (14)$$

Now we known that the output cavity should be placed at $X = 1.84$ to achieve maximum efficiency. However, this does not explain why a higher efficiency cannot be reached.

From Fig. 2 we can observe that some electrons are always away from the bunching center. These electrons will never enter the gap of output cavity at a right decelerating phase. On the contrary, they are accelerated in the output cavity, limiting the overall electron efficiency. Such electrons are called peripheral electrons or simply “outsiders”. To improve the efficiency of a klystron, the peripheral electrons should be collected into the bunching center as much as possible. This concept is important because it remains the fundamental goal of the high-efficiency bunching methods developed in recent years. In Section 4.1, we will introduce

these new bunching methods. Here, we will stick to kinematic theory of the two-cavity klystron, since it still provides beneficial concepts for high-efficiency klystron.

3.2.3. High efficiency

To achieve higher efficiency, the energy transfer from the beam to the RF should be maximized. The ideal bunching scenario for the two-cavity klystron analysis occurs when all the electrons are bunched into one phase with the maximum negative voltage as they pass through the output cavity gap. However, peripheral electrons are difficult to modulate because they require a greater phase shift to align with the bunch center.

Assuming all electron enters the output cavity at the same time, then ωt_2 should be a constant value for all the electrons. To find an ideal modulating function, the Eq. (6) is modified to

$$\omega t_2 = \omega t_1 + \frac{\omega l}{v_0\left(1+\frac{V_1(t_1)}{V_0}\right)^{\frac{1}{2}}} = \phi_0 \qquad (15)$$

The term $V_1(t_1)$ replaces $\hat{V}_1 \sin \omega t_1$ to represent the modulating wave function. Here, ϕ_0 is the constant phase for all electrons entering the output cavity. To get the ideal modulating wave function, assume that at $t_1 = 0$ and $V_1(0) = 0$. Then $\phi_0 = {}^{\omega l}/_{v_0} = \theta_0$, and Eq. (15) becomes

$$\omega t_1 + \frac{\theta_0}{\left(1+\frac{V_1(t_1)}{V_0}\right)^{\frac{1}{2}}} = \theta_0 \qquad (16)$$

The $V_1(t_1)$ is solved as

$$V_1(t_1) = V_0\left[\frac{1}{\left(1-\frac{\omega t_1}{\theta_0}\right)^2} - 1\right] \qquad (17)$$

Eq. (17) indicate that the electron modulated at $t_1 = {}^{\theta_0}/_{\omega}$ requires an infinitely high modulating voltage to catch up with the rest of the electrons. For a simpler conclusion, assuming ${}^{\omega t_1}/_{\theta_0} \ll 1$, Eq. (17) can be simplified to

$$V_1(t_1) = V_0\frac{2\omega t_1}{\theta_0}, \qquad (18)$$

$$t_1 \in \left[\frac{-\pi+2n\pi}{\omega}, \frac{\pi+2n\pi}{\omega}\right], n = 0,1,2 \ldots$$

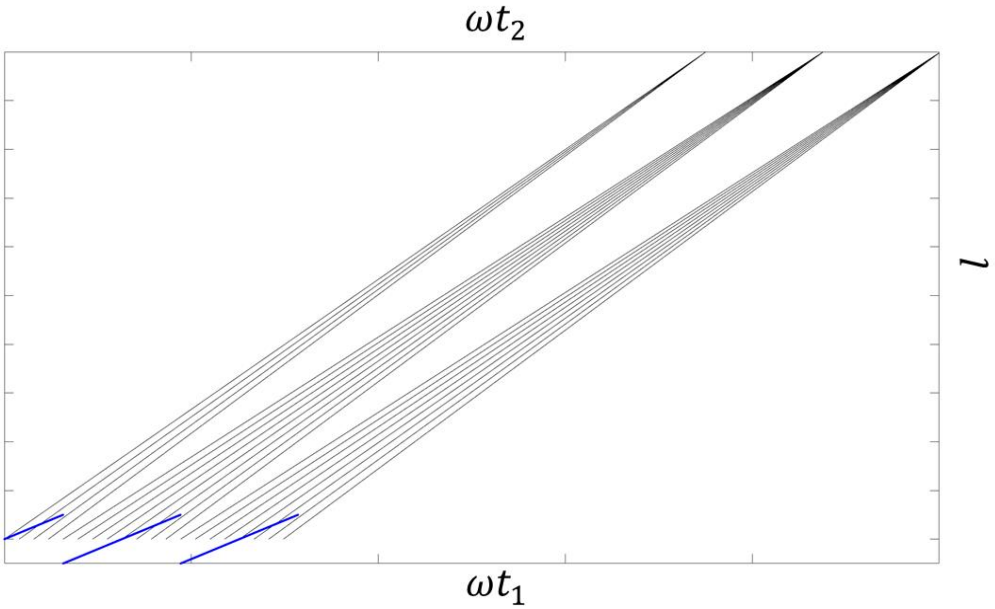

Fig. 3 The Applegate diagram with a sawtooth modulation

(The code for plotting is listed in Appendix 2)

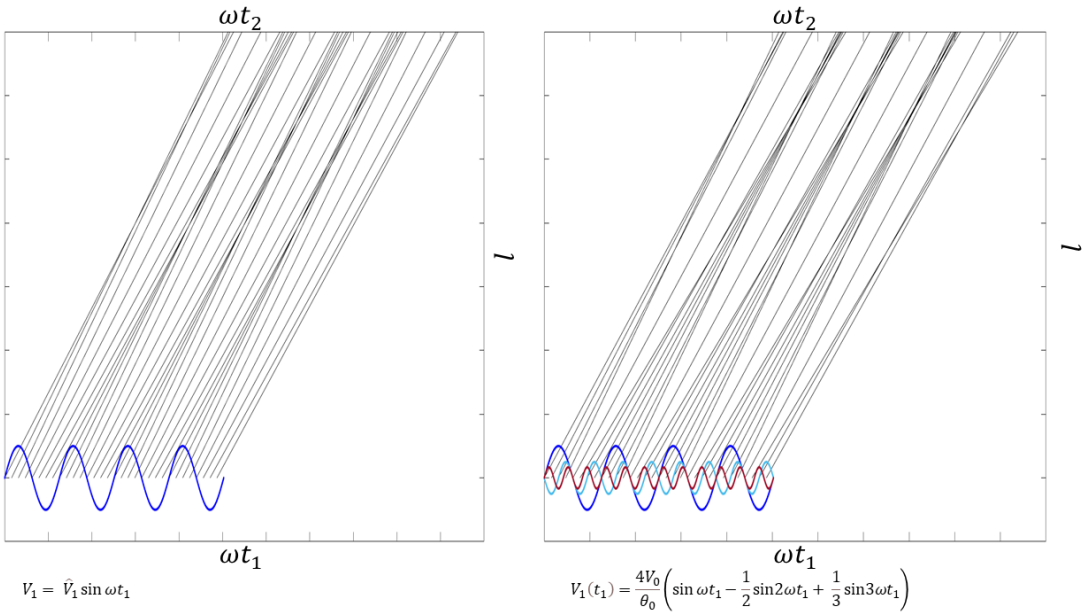

Fig. 4 Comparison of the Applegate diagrams with modulation by a fundamental sine wave vs. a serious of sine harmonics (The code for plotting the right part is listed in Appendix 3)

This means that a sawtooth function can be used as the modulating voltage to achieve ideal bunching in a two-cavity klystron.

An Applegate diagram for ideal bunching can be generated using Eq. (18) and is shown in Fig. 3. In this diagram, there are no peripheral electrons. All the electrons arrive at the output cavity at the same phase, ensuring that all the beam power is transferred to the RF.

The sawtooth voltage is difficult to realize in an RF cavity. However, the sawtooth function described by Eq. (18) can be represented as a Fourier series

$$V_1(t_1) = -\frac{4V_0}{\theta_0}\sum_{n=1}^{\infty}\frac{(-1)^n}{n}\sin n\omega t_1 \qquad (19)$$

Replacing the modulation voltage $V_1(t_1) = \hat{V}_1 \sin \omega t_1$ in Eq. (8a) with the Fourier series representation given by Eq. (19), we get

$$\omega t_2 = \omega t_1 + \theta_0 + 2\sum_{n=1}^{\infty}\frac{(-1)^n}{n}\sin n\omega t_1 \quad (20)$$

So, ideal bunching is basically formed by sine functions with frequencies that are integer multiples of a fundamental frequency. Here, we consider up to the third harmonic. Using Eq. (20) with $n = 1,2,3$, we can draw a new Applegate diagram, as shown in the right part of Fig. 4. As a comparison, the left part of Fig. 4 shows the Applegate diagram based on the Eq. (8a). The peripheral electrons are effectively reduced, demonstrating the potential for a high efficiency, by applying a combination of the fundamental, second, and third harmonics.

So far, the two-cavity kinematic theory has not included any space charge effects, which limits its applicability for designing a two-cavity. However, some concepts derived from the above discussion are still beneficial for designing a high-efficiency klystron:

1) To achieve a high-efficiency klystron, peripheral electrons should be collected into the bunching center as much as possible.
2) Bunching with harmonics improves efficiency by helping to collect peripheral electrons.

3.2.4. Space charge force

In Section 3.1, the space charge force is roughly introduced in both the transverse and longitudinal directions. The longitudinal effect

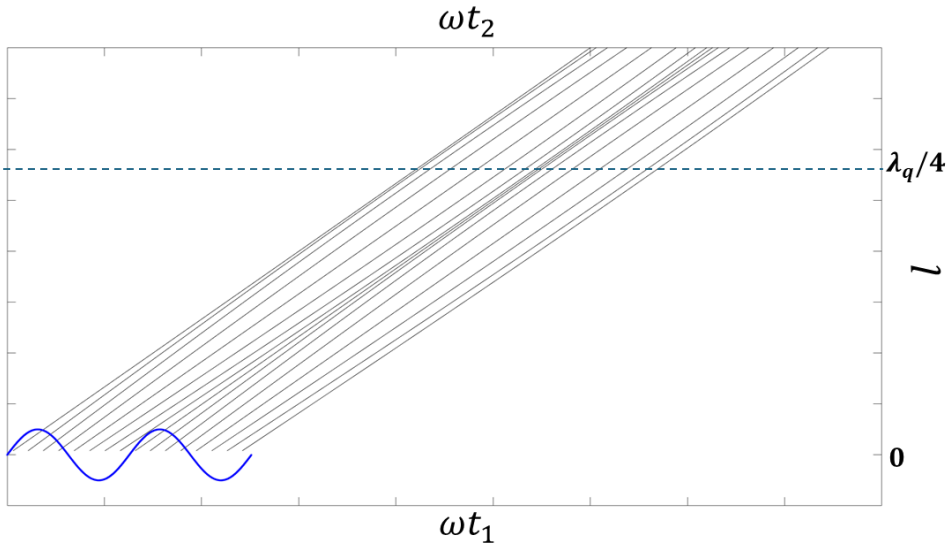

Fig. 5 The Applegate diagram with space charge effect

(The code for plotting is listed in Appendix 4)

can still be analyzed using the two-cavity kinematic theory.

Eq. (8a) and Fig. 2 provide a basic explanation of the bunching process in a two-cavity klystron. Owing to assumption 3), this equation does not contain any role of space charge force. Eq. (8a) can be modified with a factor of $\sin\beta_p l / \beta_p l$, multiplied to its 3rd term on the right [14]

$$\omega t_2 = \omega t_1 + \theta_0 - \frac{\sin\beta_p l}{\beta_p l} X \sin\omega t_1 \quad (21)$$

Where the β_p is called the plasma propagation constant, which is derived from the plasma wavelength λ_p by

$$\beta_p = \frac{2\pi}{\lambda_p} \quad (22)$$

λ_p is defined by the space charge wave theory [1][2][4]. The longitudinally modulated electron beam can be viewed as an oscillating plasma in a free space, with a wavelength of λ_p. The ω_p represent the frequency of oscillating plasma

$$\omega_p = \frac{2\pi v_0}{\lambda_p} \quad (23)$$

Considering plasma in a conductive tunnel, the plasma frequency ω_p is modified to the reduced plasma frequency ω_q by multiplying it by a plasma reduction factor R

$$\omega_q = \omega_p * R \quad (24a)$$

Similarly, the plasma propagation constant is modified to the reduced plasma propagation constant

$$\beta_q = \beta_p * R \quad (24b)$$

Then the Eq. (21) is updated

$$\omega t_2 = \omega t_1 + \theta_0 - \frac{\sin\beta_q l}{\beta_q l} X \sin\omega t_1 \quad (25)$$

An Applegate diagram based on Eq. (25) is shown in Fig. 5. Owing to the space charge force, the phase traces of electrons are bent. When the current density is high or the modulation voltage is low, the electrons are pushed back before they can overtake each other [14]. This illustrates an intuitive image of the "anti-bunch effect" caused by the space charge force. Fig. 5 shows that the length over which the bunch core is formed is a quarter of the reduced plasma wavelength $\lambda_q/4$.

The beam (micro) perveance μP is an important parameter that indicates the magnitude of the space charge effect in a beam

$$\mu P = 10^6 \frac{I_0}{V_0^{3/2}} \quad (26)$$

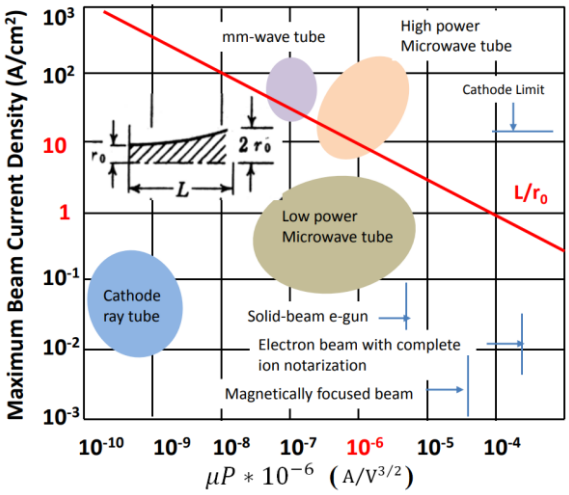

Fig. 6 [17] Distribution map represented by beam perveance and maximum beam current density

There is an inverse relationship between the beam perveance and the efficiency in the field of klystron: lower perveance corresponds to higher efficiency [16]

$$\eta = 78 - 16 \times \mu P \qquad (27)$$

This empirical formula is widely used to demonstrate the relationship between efficiency and perveance in klystrons.

The beam perveance is of great importance in the wider usage of vacuum devices involving electron beams. Fig. 6 [17] demonstrates a distribution map with beam perveance on the horizontal axis and maximum beam current density on the vertical axis. It characterizes the space charge force and is deeply related to the bunching formation and, therefore, to efficiency [17].

From Fig. 6, we can see that microwave tubes (klystron, IOT, TWT, etc.) are located in a region with a perveance range from 10^{-7} to 10^{-6} $A/V^{3/2}$ and a maximum beam current density from 10^{-1} to 10^{2} A/cm^2. Other types of electric vacuum devices that are not related to high-power sources, such as cathode ray tubes or the electron guns of linacs, locate in different ranges.

Transverse expansion is not considered in the one-dimensional analysis discussed previously. However, the straight line L/r_o in Fig. 6 explains the transvers space charge effect of an electron beam. The beam with an original radius of r_o expands to a radius of $2r_o$ after drifting a length of L. This line illustrates that the beam perveance has a strong relationship to the extent of transvers space charge force.

The space charge effect is the most dominating factor influencing the new bunching methods. Due to its complexity, computer simulation is the most reliable tool for designing a high-efficiency klystron.

3.3. Disk model simulation

Numerical simulation plays a crucial role in precisely designing a klystron. The one-dimensional disk model programs are among the most popular simulation tools, such as JPNDISK [18], AJDISK [19], among others.

The disk model program divides the electron beam into multiple electron layers, which is considered as a "hard disk". All electrons within the disk undergo the same longitudinal motion, while transverse motion is not considered. The

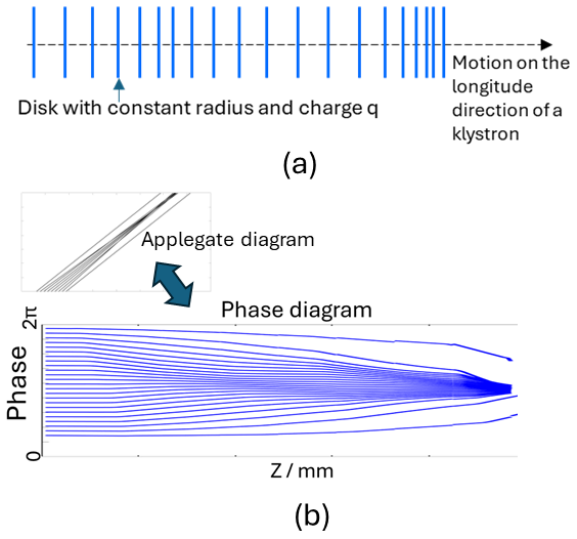

Fig. 7 (a)Schematic of a disk model, (b) Example of a phase diagram from a disk model simulation

space charge force is treated as electric forces between those disks.

Fig. 7 illustrates a schematic of the disk model and an example of a phase diagram resulting from a disk model simulation. The Applegate diagram, frequently used to present the electron phase trace in previous discussions, is also a key result of the disk model simulation. A slight difference is that it is usually presented horizontally in the disk model simulation results.

In Section 4.1, input data and outcome result of the disk model simulation will be provided for a direct understanding of the simulation process for a high-efficiency klystron.

3.4. Particle in Cell simulation

The most sophisticated tool for klystron design is the Particle-in-Cell (PIC) simulation. In PIC simulation, particles are tracked in space through time at discrete time intervals, while electromagnetic fields are timely computed at discrete locations. The particle in the PIC is the so called "macroparticle", which represents many real particles [20].

As a general-purpose solver for Maxwell's equations and electron motion equation, the PIC simulation allows for applying a realistic 2D/3D boundary. This capability provides a method to design a realistic klystron. Additionally, PIC simulation can predict spurious oscillations caused by high order modes.

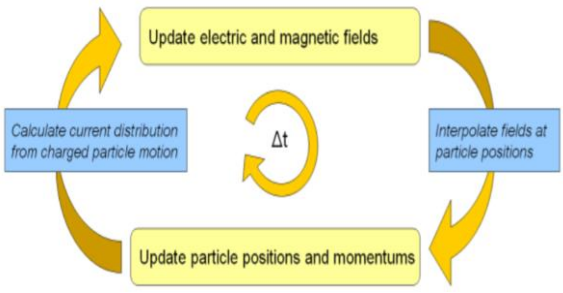

Fig. 8 [21] The updating scheme of CST PIC solver

The PIC or quasi-PIC programs that can be used for klystron design include CST [21], EMSYS [22], and others. Fig. 8 [21] illustrates the scheme of the PIC solver for updating the electromagnetic field and particle positions and momentums at time steps. An example of PIC simulation will be presented in Section 5.2.

4. High-efficiency klystron

4.1. New Bunching Methods

So far, most efforts have focused on improving the cavity layout of the RF-beam interaction section. New bunching methods can enhance the efficiency of klystrons.

In 1974, the concept of congregated bunching [23] was introduced. This one-dimensional assumption suggests that for a klystron to achieve high efficiency, the electrons entering the output cavity must have a specific velocity distribution. It claimed that electrons entering the output cavity gap earlier should be slower than those entering later. Some research [23] indicate that a theoretical ultimate efficiency of 90% could be reached based on this assumption. However, this assumption is hardly helpful for generate any specific method for forming the ideal bunch.

In recent years, several new bunching methods and ideas have been proposed to improve klystron efficiency, including:

1) Core Oscillation Method (COM) [24]

The main principle of COM is that after the electron beam is velocity modulated by the cavity, electrons at the bunching center repel each other due to space charge forces, creating a gentle core oscillation. Meanwhile, peripheral electrons slowly approach the bunching center. After several core oscillation processes, the peripheral electrons can get close enough to the

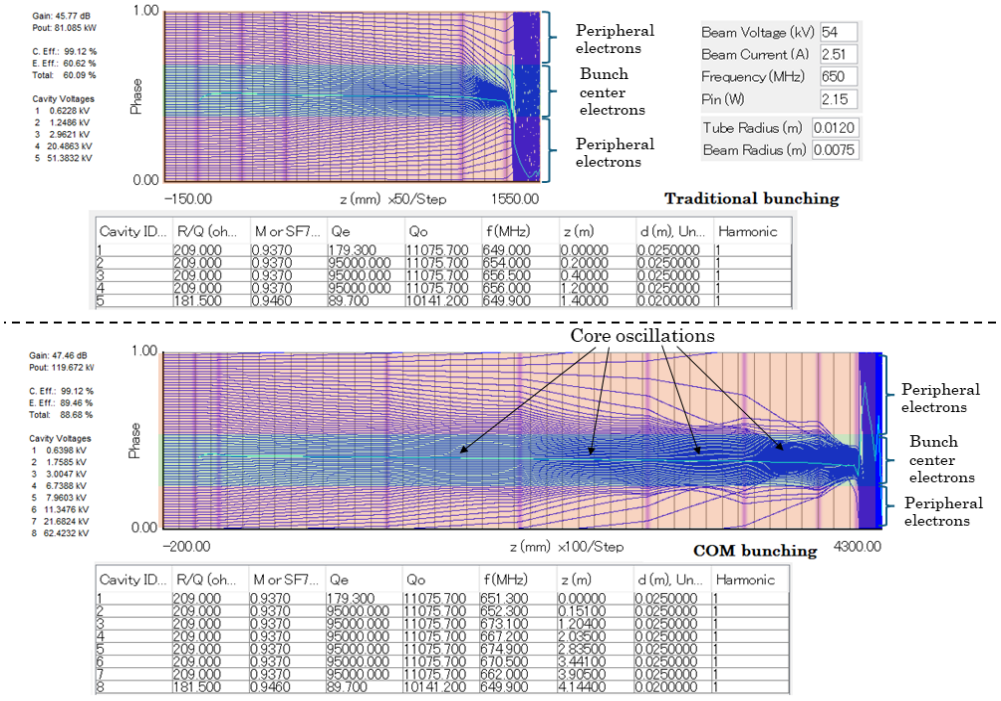

Fig. 9 Simulation comparison of traditional bunching and COM using AJDISK

bunching center and enter the output cavity, converting more electron energy into microwave energy, thus increasing the klystron's efficiency.

Fig. 9 illustrates the principle of COM compared to traditional bunching using the AJDISK code. Similar to the Applegate diagram, a disk model code presents the phase diagram of the disks. Input data for the AJDISK code is also shown in Fig. 9 for those interested in conducting the simulation independently. In traditional bunching, only the central region electrons can enter the decelerating phase of the output cavity, while a lot of peripheral electrons, unable to gather at the center, do not convert their energy into microwave energy and instead are accelerated in the output cavity gap. Traditional bunching limits klystron efficiency by actively abandoning peripheral electrons. COM, through multiple core oscillation processes, allows peripheral electrons to slowly gather into the phase range of bunch center. COM requires each resonant cavity to modulate the electron velocity lightly, ensuring that the bunching center does not oscillate too strongly, causing severe electron surpassing. This allows for controlled velocity modulation and repeated core oscillation. Since the fundamental resonant cavity naturally limits the velocity modulation voltage for peripheral electrons, they need multiple times of modulations and a long-distance drift to approach the bunch center phase region. Consequently, the interaction section length required by COM is relatively long, far exceeding the length of all existing klystrons.

2) Bunching-Alignment-Collecting (BAC) [25]

BAC method is an improvement on COM that uses additional resonant cavities to accelerate the core oscillation process, thereby shortening the interaction section length. The additional cavities are designated for Bunching, Alignment, and Collection. The Bunching cavity typically uses a fundamental resonant cavity to achieve electron bunching. The Alignment cavity corrects the velocity of the bunching center electrons, reducing speed dispersion [25]. It is usually tuned below the operating frequency of the klystron. The Collecting cavity,

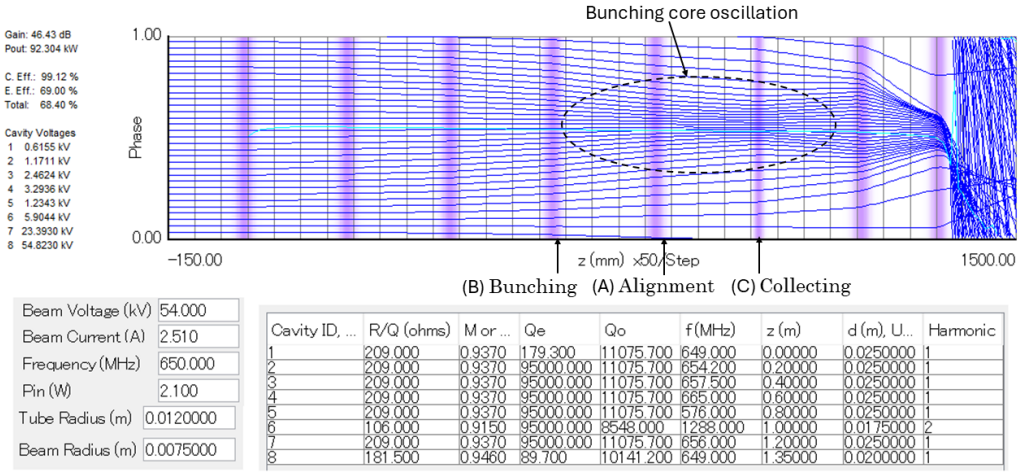

Cavity ID, ...	R/Q (ohms)	M or ...	Qe	Qo	f (MHz)	z (m)	d (m), U...	Harmonic
1	209.000	0.9370	179.300	11075.700	649.000	0.00000	0.0250000	1
2	209.000	0.9370	95000.000	11075.700	654.200	0.20000	0.0250000	1
3	209.000	0.9370	95000.000	11075.700	657.500	0.40000	0.0250000	1
4	209.000	0.9370	95000.000	11075.700	665.000	0.60000	0.0250000	1
5	209.000	0.9370	95000.000	11075.700	676.000	0.80000	0.0250000	1
6	106.000	0.9150	95000.000	8548.000	1288.000	1.00000	0.0175000	2
7	209.000	0.9370	95000.000	11075.700	656.000	1.20000	0.0250000	1
8	181.500	0.9460	89.700	10141.200	649.000	1.35000	0.0200000	1

Fig. 10 Simulation of BAC method using AJDISK

typically a second harmonic cavity, exerts a strong bunching effect on peripheral electrons, quickly moving them to the bunching center. Fig. 10 shows the phase diagram using BAC method from the AJDISK code, with specific input data provided. Fig. 10 demonstrates the effective collection of peripheral electrons using BAC method. The Alignment cavity mitigates the anti-bunching effect at the bunching center, maintaining phase relationships despite strong space charge forces.

Due to its independence from perveance limitations and control over the length of the interaction section, the BAC bunching method has been widely adopted in practice. The efficiency of S-band klystrons using this bunching method has exceeded 60%. The detailed information will be presented in Section 5.1.

3) Core Stabilization Method (CSM) [26]

CSM employs second and third harmonic cavities to rapidly incorporate peripheral electrons into the bunching center while reducing the space charge forces at the bunching center. Similar to BAC method, CSM uses a second harmonic and third harmonic cavity to strongly bunch peripheral electrons. From another aspect, CSM uses harmonic cavities to create internal sub-bunches within the bunching center, reducing the anti-

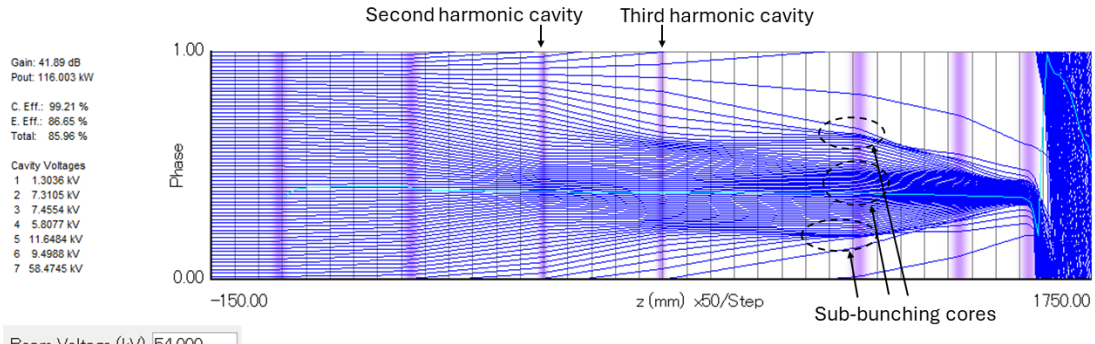

Cavity ID,...	R/Q (ohms)	M or ...	Qe	Qo	f (MHz)	z (m)	d (m), Un...	Harmonic
1	209.000	0.9370	165.100	11075.700	650.500	0.00000	0.0250000	1
2	209.000	0.9370	95000.000	11075.700	652.100	0.28400	0.0250000	1
3	106.000	0.9150	95000.000	8548.000	1293.300	0.56800	0.0175000	2
4	72.800	0.8500	95000.000	6916.500	1941.800	0.82300	0.0140000	3
5	209.000	0.9370	95000.000	11075.700	667.600	1.25000	0.0250000	1
6	209.000	0.9370	95000.000	11075.700	679.300	1.46700	0.0250000	1
7	181.500	0.9460	81.200	10141.200	650.100	1.61700	0.0200000	1

Fig. 11 Simulation example of CSM using AJDISK

bunching effect and stabilizing the bunching core to some extent. Fig. 11 is a simulation example of CSM using AJDISK, with all the input data provided. Fig. 11 shows that peripheral electrons move increasingly faster towards the bunching center after modulation by the fundamental, second, and third harmonic cavities. Due to the third harmonic bunching, three sub-bunching cores form in the bunching center. When the bunching center electrons meet peripheral electrons at the penultimate cavity, most electrons have already entered the effective phase range of the cavity. Without these sub-bunching cores, the bunching center electrons would undergo severe oscillation, stopping peripheral electrons from moving towards the bunching center.

CSM is primarily suitable for L-band or UHF-band klystrons, where the drift tunnel diameter can be selected for a relatively high cut-off frequency (at least higher than the third harmonic cavity frequency). Additionally, CSM is suitable for low-perveance electron beams.

4) Adiabatic Bunching [27]

Adiabatic Bunching, also known as Kladistron, is a method that completes the entire bunching process through numerous low characteristic impedance resonant cavities. Each cavity has a low cavity voltage, resulting in minor velocity modulation for the electrons. This causes the the fundamental component of AC current in the electron beam to grow slowly.

Due to the changes in external bunching forces being much slower than the changes in the internal space charge forces within the electron beam, it is like a quasi-adiabatic state, hence it is called adiabatic bunching [27]. This bunching process is similar to that in a Radio Frequency Quadrupole (RFQ) [27], which is used in proton linacs to bunch, focus, and accelerate a continuous beam from keV to MeV [27].

Fig. 12(a) [27] is a phase diagram from a disk model simulation. A total 20 cavities are used for the layout. Peripheral electrons are slowly gathered into the benching center, while the bunching center does not show any clear oscillation, which is different from the COM. Fig. 12(b) [27] shows an RFQ cavity and the phase diagram of protons in an RFQ cavity. These two types of phase diagrams demonstrate the bunching status in a similar sense.

5) Two-stage method [28]

The two-stage method adopts two DC accelerating gaps for a klystron, which usually has only one. This approach allows for achieving an ultra-low beam perveance after the second acceleration. As a result, a high efficiency could be reached while the length of the klystron is much shorter than a traditional klystron with a constant low beam perveance (The plasma wavelength λ_p has an inverse relationship with the beam perveance μP). However, this significant retrofit introduces new technical challenges, including:

a) RF feed to the input cavity on the high voltage state.

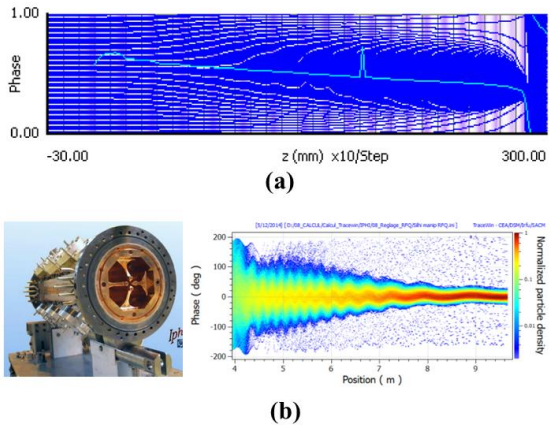

Fig. 12 [27] (a) Phase diagram from a disk model simulation of an Adiabatic Bunching, (b)The RFQ cavity and the phase diagram of protons in an RFQ cavity

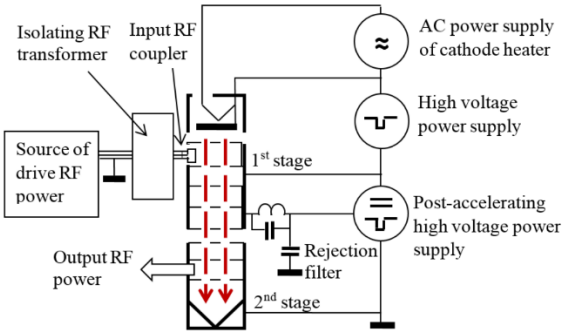

Fig. 13 [28] The conceptualization of the two-stage klystron

b) Insulation of the second accelerating gap while preventing the RF leak.

c) Beam focusing magnet that accommodate the two-stage structure.

The conceptualization of a two-stage klystron is shown in Fig. 13 [28]. It has incorporated two accelerating gaps. The beam is emitted from the electron gun with a high perveance and bunched by the cavities located on the high-voltage potential. Then the bunched beam passes through the post-accelerating gap. Since the 2nd accelerating voltage is 4~5 times higher than the 1st one, a dramatic decrease of beam perveance releases the space-charge force and the anti-bunching effect. Then the following penultimate cavities could effectively squeeze the bunch before it enters the output cavity.

4.2. Depressed collector [29]

The depressed collector is used to enhance the overall efficiency of a klystron. Unlike a normal collector, where the spent beam hits the wall and dissipates heat, the depressed collector aims to recover the power of the spent beam and convert it back into electrical power.

4.3. Advantages of an MBK

According to the number of electron beams, klystrons can be divided into two major categories: single-beam klystrons (SBK) and multi-beam klystrons (MBK). The single-beam klystron is the most common type, characterized by its simple structure and wide range of applications. In contrast, the multi-beam klystron, which requires multiple cathodes to emit electron beams, has a more complex overall structure. However, MBK has greater potential for high efficiency.

According to Eq. (27), an overall parameter design of high-efficiency klystron will necessarily minimize the perveance. A lower perveance generally requires a higher voltage for the electron gun. However, excessively high electron gun voltage can negatively affect the operational stability of the klystron. In contrast, for an MBK, the electron gun voltage is significantly lower for the same output power, efficiency, and perveance compared to a single-beam klystron.

As shown in Table 3, for a klystron with an output power of 80 MW and an efficiency of 70%, if the desired perveance is 0.29 $\mu A/V^{3/2}$, the electron gun voltage of a single-beam klystron is as high as 689 kV. While the electron gun voltage of an 8-beam MBK is 300 kV, which is acceptable for a pulsed klystron. Therefore, an MBK can achieve extremely low perveance while maintaining the electron gun voltage within a reasonable range. Since reducing the perveance of the electron beam to improve klystron efficiency has become unavoidable, the MBK will show significant advantages in the field of high-efficiency klystron.

Table 3 Comparison of perveance and beam voltage between SBK and MBK

Output power (MW)	80	80
Efficiency	70%	70%
Total beam power (MW)	114.3	114.3
Number of beams	1	8
Perveance ($\mu A/V^{3/2}$)	0.29	0.29
Electron gun voltage (kV)	689	300

The relationship between the electron gun voltage and the number of electron beams of an MBK is expressed by the following formula

$$V_0 = \left(\frac{P_1}{\eta N_b \mu P * 10^{-6}}\right)^{\frac{2}{5}} \quad (28)$$

where N_b is the number of electron beams. Eq. (28) and Table 3 both indicate that the MBK can simultaneously achieve the dual advantages of low perveance and acceptable electron gun voltage.

5. Global research activities

5.1. The existing high-efficiency klystrons

The E37503 MBK developed by CANON has achieved an efficiency of 71.5% [30], with an operating frequency of 999.516 MHz, 6 electron beams, individual beam perveance of 0.42 $\mu A/V^{3/2}$, and an output peak power of 20.5 MW. The RF pulse width and repetition frequency are 150 ms and 25 Hz, respectively. The E37503 was developed for the CLIC. For the same project, Thales developed the TH1803 MBK, which adopts 10 electron beams, with individual beam perveance of 0.34 $\mu A/V^{3/2}$, an output power of 21 MW, and an efficiency of 73.5% [31]. The VDBT of Russia developed a series of S-band MBKs using the BAC bunching method, all with efficiencies above 60% [32]. The BT267 in this series achieves a peak output power of 16 MW and an average power of 30 kW.

Earlier high-efficiency klystron was developed for space power application. In the 1970s, the CPI developed the single-beam S-band klystron VKS-7773 [33]. Its beam perveance is 0.521 $\mu A/V^{3/2}$. It has a CW output power of 50 kW, and an efficiency of 74.4%. The beam voltage and current are 28 kV and 2.4 A, respectively. For the high-power requirements in the particle accelerator field, CPI developed the UHF band CW single-beam klystron VKP7952A, which achieved an output power of 1 MW and an efficiency of 65% [34].

Some high-peak-power single-beam klystron initially used in linear accelerators have been modified to improve efficiency. In 2016, SLAC attempted to use the BAC bunching method to increase the efficiency of 5045 klystron from 45% to 60% without changing the klystron length [35]. The actual measured efficiency was 54%. However, due to high-order mode oscillations within the klystron, the output microwave pulse width was limited to 0.1 μs [36].

Table 4 The existing high-efficiency klystrons worldwide

Frequency band	Vendor / Type	Frequency (GHz)	Peak power (MW)	Average power (MW)	MBK or SBK	Efficiency	Perveance ($\mu A/V^{3/2}$)	Beam voltage (kV)
S-Band	VDBT / BT267	2.856	16	0.03	MBK	60%	0.51	75
	SLAC / 5045(retrofit)	2.856	72		SBK	54%	2	350
	CANON / E3772A(retrofit)	2.856	7.3		SBK	59.2%	1.68	140
	CPI / VKS-7773	2.45	0.05	0.05	SBK	74.4%	0.51	28
L-Band	CANON / E37503	1	20.5	0.077	MBK	71.5%	0.42	160
	Thales / TH1803	1	21	0.079	MBK	73.5%	0.34	147
	CANON / E3736	1.3	10	0.15	MBK	65%	0.56	115
	Thales / TH1801	1.3	10	0.15	MBK	65%	0.51	110
	CPI / VLK8301B	1.3	10	0.15	MBK	65%	0.57	115
UHF-Band	CPI / VKP7952A	0.7	1	1	SBK	65%	0.6	92
	CANON / E3786	0.509	1.2	1.2	SBK	65%	0.74	93

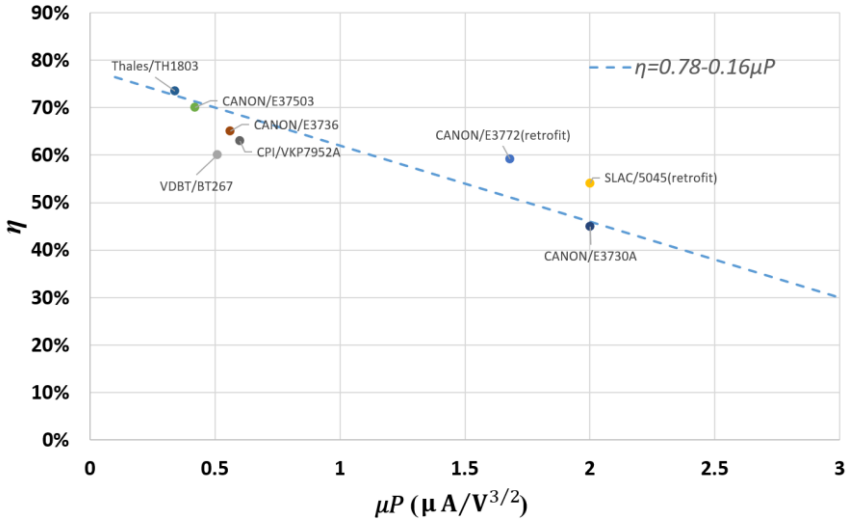

Fig. 14 Plot of the empirical formula illustrating the relationship between perveance and efficiency

CANON modified the E3772A klystron used in medical accelerators to enhance its efficiency [30]. The E3772A operates at a frequency of 2856 MHz, with a peak output power of 7.5 MW, and an efficiency of 45%. Without changing the length of the high-frequency interaction section, the number of resonant cavities was increased from 5 to 10. A high-efficiency prototype tube was measured with an efficiency of 59.2% [30]. Table 4 lists the technical parameters of existing high-efficiency klystrons worldwide. Fig. 14 shows the plot of Eq. (27), with the data points for existing klystrons marked. The horizontal axis represents perveance, while the vertical axis represents efficiency.

5.2. Research activities at KEK [37]

As introduced in Section 2.2, an S-band high-efficiency MBK is currently under development to modernize the existing 50MW klystron utilized in the KEK e^-/e^+ Injector Linac. With an emphasis on energy conservation, the RF-section of this MBK is designed to achieve a target efficiency of 73%, a significant improvement over the efficiency 45% of the current 50 MW klystron. Fig. 15 is a snapshot of bunched beams inside the 80MW MBK (KMS80) from CST, resulting from the PIC

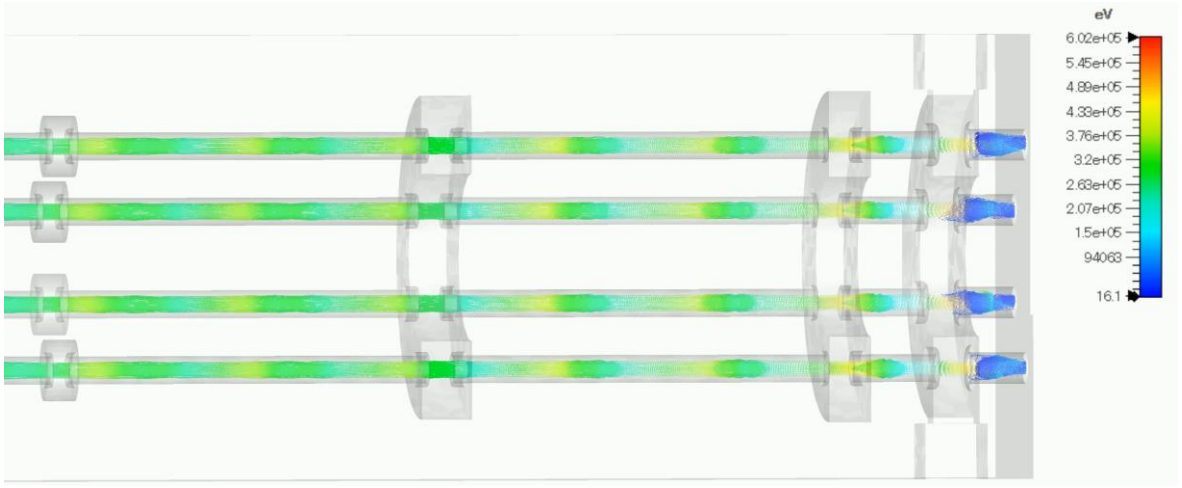

Fig. 15 The 80MW MBK from CST

simulation. The color bar represents the particle energy. From the left to the right, the individual second harmonic cavities, two penultimate cavities, and the output cavity with two coupled waveguides are shown in Fig. 15. Beams are gradually formed to bunches when they drift through the tunnels and reach the output cavity, indicating an effective beam density modulation. Table 5 lists the main parameters of the KMS80.

Table 5 Main parameters of the KMS80

Parameters	value
Frequency (MHz)	2856
Gun voltage (kV)	300
Total gun current (A)	366.4 (45.8*8)
Beam No.	8
Output power (MW)	80
Efficiency	73%

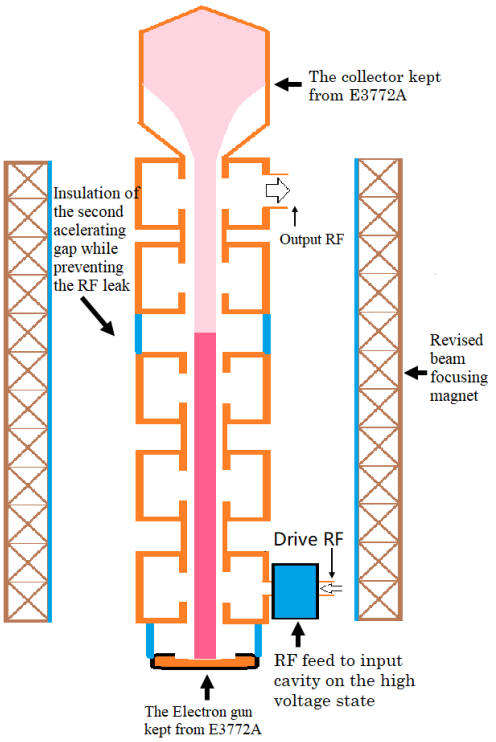

Fig. 16 The schematic illustration of the two-stage klystron retrofitted from the existing S-band klystron.

Based on a 7.5 MW klystron E3772A from CANON, a S-band two-stage klystron is under development. The purpose is to design a two-stage klystron based on an S-band klystron and then modify it to verify the new design. Fig. 16 shows the schematic illustration of the S-band two-stage klystron. The newly designed two-stage klystron would keep the existing structures of the electron gun and the collectors to minimize development costs. New structures, such as insulation for the drive-RF feeding, the post-accelerating gap, and revised focusing solenoids, among others, are added to the design. Table 6 lists the main parameters of the newly designed two-stage klystron, compared with those of the E3772A.

Table 6 Main parameters of the E3772A and two-stage klystron

Parameters(unit)	E3772A	Two-stage klystron (design)
Efficiency	45%	72%
Frequency (GHz)	2.856	2.856
Beam voltage (kV)	150	80 (gun)+170 (post accel. gap)
Beam current (A)	110	41
Output power (MW)	7.5	7.5
Cavity number	5	6
Length (m)	1	1

The efficiency of the existing S-band klystron is improved from 45% to 72%, with keep a same output power and klystron length. The total voltage is limited to 250 kV to ensure that the prototype can be tested on the existing test-stands.

5.3. Research activities at CERN [38]

CERN collaborating with CANON, is developing the X-band high-efficiency klystron. The prototypes are based on CANON E37113 [40]. The efficiency is improved from 39% to 56% by testing several protypes. Table 7 lists the parameters of the E37113 and newly developed high-efficiency (HE) prototype.

Table 7 Parameters of the E37113 and high-efficiency prototype

Parameters(unit)	E37113	HE E37113
Efficiency	39%	56%
Frequency (GHz)	11.994	11.994
Beam voltage (kV)	157	153
Beam current (A)	96	93
Output power (MW)	6	8

It has been reported that the first and second prototypes encountered instabilities due to high-order modes and detuning of the output coupler, respectively. After making modifications, the third prototype achieved an efficiency of 56% with an output power level of 8 MW.

A CW UHF-band klystron is under development as a spare unit for the TH2169 Thales, which operates at the Large Hadron Collider (LHC). The designed efficiency of the new klystron is improved from 62% to 70 %, while adhering to restrictions on gun voltage and length. Table 8 lists the parameters of TH2169 and the newly designed high-efficiency (HE) TH2169.

Table 8 Parameters of the TH2169 and HE TH2169

Parameters (unit)	TH2169	HE TH2169
Efficiency	62%	70%
Frequency (MHz)	400.8	400.8
Beam voltage (kV)	58	58
Beam current (A)	8.4	9
Output power (kW)	300	365

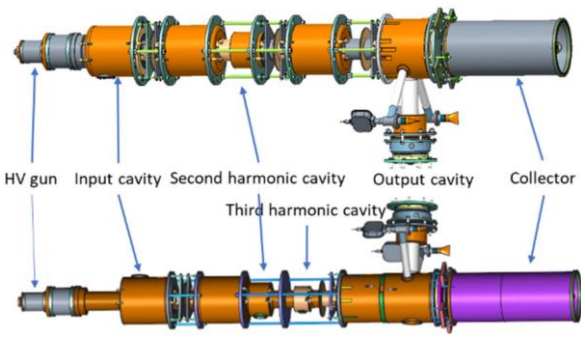

Fig. 17 [38] The TH2169 and HE TH2169

Fig. 17 [38] shows the configurations of the TH2169 and HE TH2169. Fig. 17 illustrates that the HE TH2169 tube has adopted the CSM bunching method.

For the future FCC project, CERN presents a design of a CW UHF-band MBK operating at 400MHz and an output level of 1 MW. The design adopts the two-stage technology and the efficiency from simulation is 82%. The length of the MBK is 3m, considered as a compact structure. Fig. 18 [38] shows the configuration of the 0.4 GHz two-stage MBK.

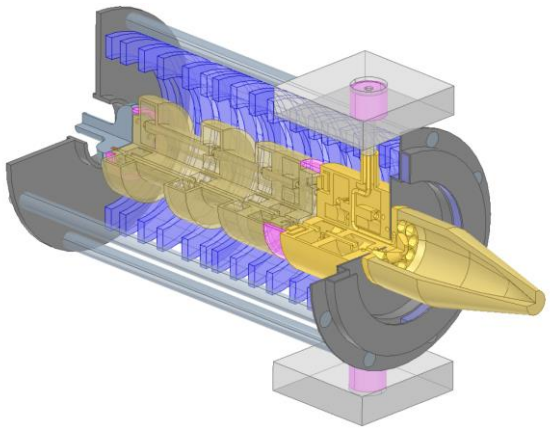

Fig. 18 [38] The 0.4 GHz two-stage MBK

5.4. Research activities at CEA [39]

CEA, with a collaboration of Thales, has developed a klystron prototype adopting the Adiabatic Bunching method. The Thale TH2166 was chosen for retrofitting as a demonstration of the Adiabatic Bunching. The original 6 cavities were increased to 16 cavities. While the input and output cavities are retained, the intermediate 14 cavities have low R/Q and weak coupling with the beam, to accomplish a serous of slow and soft bunch to the beam. The prototype was tested, with the highest measured efficiency at 41%, compared to the 50% efficiency of the TH2166. The drop of efficiency is primarily due to discrepancies between the actual layout parameters and the designed parameters, particularly the cavity

frequencies. These issues arose from cavity deformation during fabrication and malfunction of the tuning mechanisms. In addition to the frequency shifts, an oscillation near 4.96 GHz was observed in the output signal spectrum. Table 9 lists the parameters of the design parameter and measurement results.

Table 9 Parameters of the TH2166 and Adiabatic Bunching prototype

Parameters	TH2166	New prototype	
		Design	Test
Efficiency	50%	60%	41%
Frequency (GHz)	4.9	4.9	4.9
Beam voltage (kV)	26	26	27.8-30
Beam current (A)	4.3	4.3	

5.5. Research activities at CPI [41]

CPI is developing an X-band 50MW high-efficiency klystron. With assistance from CERN and improvements made independently, CPI proposed a design in 2022 that achieves over 60% efficiency in simulations. The second harmonic cavities and multi-cell output cavity are used to improve the efficiency. Table 10 lists the main parameters of the design.

Table 10 Parameters of the CPI 50 MW klystron

Parameters	value
Efficiency	>60%
Frequency (GHz)	11.994
Beam voltage (kV)	400
Beam current (A)	190
Output power (MW)	52

5.6. Research activities at Calabazas Creek Research Inc. [42]

Calabazas Creek Research Inc. is developing an L band CW klystron with an output power of 100 kW. Table 11 lists the simulation parameters. The COM bunching method is adopted for this design.

Table 11 Parameters of the L-band 100 kW klystron

Parameters	value
Efficiency	79%
Frequency (GHz)	1.3
Beam voltage (kV)	53.5
Beam current (A)	2.46
Output power (kW)	100

5.7. Research activities at IHEP [43]

IHEP has proposed designs of high-efficiency UHF-band CW klystrons with output level of 800 KW for the CEPC project. Both single beam and multi-beam design are launched. Table 12 lists the parameters of the design. The CSM bunching method is adopted to improve efficiency, meaning that both second harmonic and third harmonic cavities are used in the RF section. Fig. 19 [43] shows the configuration of the 650 MHz / 800 kW MBK.

Table 12 The parameters of HE klystron for CEPC

Parameters	MBK	SBK
Efficiency	80%	78%
Frequency (MHz)	650	650
Beam voltage (kV)	54	110
Beam current (A)	20.8 (2.51×8)	9.1
Output power (kW)	800	800

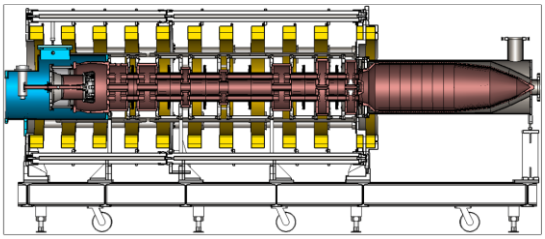

Fig. 19 [43] The MBK for the CEPC project

6. Summary

This lecture introduces the motivation, background, and impact of enhancing klystron

efficiency. It is followed by a discussion of the basics of a klystron, highlighting concepts critical to high-efficiency klystron design. Various methods for improving klystron efficiency are reviewed, and the global research landscape in this field is also presented.

7. Reference

[1] S. Fukuda, OHO 1988

[2] S. Michizono, OHO 2002

[3] S. Matsumoto, OHO 2017

[4] G. Caryotakis, High Power Klystrons: Theory and Practice at the Stanford Linear Accelerator Center, SLAC-PUB 10620

[5] S. Fukuda, et al., Design and evaluation of a compact 50 MW RF source of the PF linac for the KEKB project, Nuclear Instruments and Methods in Physics Research. A, 1996

[6] A. Jensen, et al, 25 Year Performance Review of the SLAC 5045 S-Band Klystron, Proceedings of IPAC2011, San Sebastián, Spain

[7] D. Sprehn, et al, The Design and Performance of 150 MW S-band klystons, SLAC-PUB-6677

[8] S. Isagawa, et al, Development of High Power CW Klystrons for TRISTAN, PAC1987

[9] T. Shidara, OHO 1990

[10] ILC Technical Design Report, Volume 3 – Accelerator Part II: Baseline Design.

[11] Energy Efficiency (https://fcc.web.cern.ch/energy-efficiency)

[12] A Grudiev, 380 GeV CLIC power consumption, Workshop on efficient RF sources, 2022

[13] J. Gao, CEPC Accelerator TDR Status and AC Power Consumptions, JACoW eeFACT2022

[14] J. Xie, Y. Zhao, Bunching Theory of Klystron, Science Publishing 1966

[15] MATLAB and Statistics Toolbox Release 2022b, The MathWorks, Inc., Natick, Massachusetts, United States

[16] A, Beunas, et al, A high power long pulse high efficiency multi beam klystron. 5th MDK Workshop, 2001

[17] S. Fukuda, ILC School-High Efficiency RF Source

[18] H. Yonezawa, et al, One-dimensional disk model simulation for klystron design, SLAC-TN-84-5

[19] A. Jensen, et al, Developing sheet beam klystron simulation capability in AJDISK, SLAC-PUB-15879

[20] Particle-in-cell (https://en.wikipedia.org/wiki/Particle-in-cell)

[21] CST Studio Suite Help Document (https://www.3ds.com/products/simulia/cst-studio-suite)

[22] T. Shintake, Klystron simulation and design using the field charge interaction (FCI) code, Nuclear Instruments and Methods in Physics Research. A, 1995.

[23] A. Y. Baikov, et al, Toward High-Power Klystrons With RF Power Conversion Efficiency on the Order of 90%, IEEE Transactions on Electron Devices, 2015

[24] A. Y. Baikov, et al, Simulation of conditions for the maximal efficiency of decimeter-wave klystrons. Technical Physics, 2014

[25] I. A. Guzilov, BAC method of increasing the efficiency in klystrons. IEEE Vacuum Electron Sources Conference (IVESC), 2014.

[26] C. Victoria, et al, Particle-in-Cell simulation of the third harmonic cavity F-tube klystron. IEEE International Vacuum Electronics Conference (IVEC), 2016

[27] F. Peauger, High efficiency–high perveance Klystron (X-band). EnEfficiency RF sources Workshop, 2014

[28] V. E. Teryaev, et.al, Innovative Two-Stage Multibeam Klystron: Concept and Modeling. IEEE Transactions on Electron Devices, 2020

[29] A. Staprans, et.al, High-power linear-beam tubes, Proceedings of the IEEE, 1973

[30] T. Anno, CETD experience with high efficiency S-band klystrons, CLIC Workshop 2019

[31] S. Döbert, High-efficiency L-band klystron development for the CLIC Drive Beam, CLIC workshop 2018

[32] I. Guzilov, VDBT BAC MBK Klystrons Family Status report, CLIC Workshop 2019

[33] A. D. Larue, High efficiency klystron CW amplifier for space power applications, 1976 International Electron Devices Meeting, 1976

[34] S. Lenci, et.al, Recent Progress in CW Klystrons at CPI, Proceedings of LINAC 2002

[35] A. Jensen, et al, Increasing klystron efficiency using COM and BAC tuning and application to the 5045 Klystron, IEEE International Vacuum Electronics Conference (IVEC), 2016.

[36] R. Kowalczyk, et al, Test of a BAC klystron. SLAC-PUB-17102.

[37] T. Natsui, et al, Design of The Gun and The Magnet for S-Band 80 MW Multi-Beam Pulsed Klystron, Proceedings of the Annual Meeting of Particle Accelerator Society of Japan, 2024

[38] N. C. Lasheras, et al, High-Efficiency Klystrons from A Dream to A Reality, 15th International Particle Accelerator Conference, 2024

[39] J. Plouin, et al, Design, Fabrication, and Test of a 5 GHz Klystron Based on the Kladistron Principle, IEEE Transactions on Electron Devices, 2023

[40] T. Anno, X-band High Efficiency Klystron Development, Workshop on Efficient RF Sources, 2022

[41] T. Kimura, High Efficiency 50MW X-band Klystron Development, Workshop on Efficient RF Sources, 2024

[42] M. Read, et al, A 1.3 GHZ 100 kW Ultra-High Efficiency Klystron, IEEE International Conference on Plasma Science (ICOPS), 2018

[43] S. Wang, et al, Design study and modeling of multi-beam Klystron for Circular Electron Positron Collider, Nuclear Instruments and Methods in Physics Research. A, 2022

8. Appendix

1.MATLAB code for plotting Applegate diagram in Fig. 2

```
fclose all;
clear;
omega_rf = 2 * pi * 2856000000;            %%%%%%MHZ
DCbeam_voltage = 350000;                   %%%%%kV
v0 = 239141636.9;                          %%%%%%m/s
L = 0.35;                                  %%%%%%meter
alfa = 0.15;                               %%%%%% alfa = V_1/V_0
h = 10;                                    %%%%%% number of period
Res = 4;                                   %%%%%%%%%sample number
omega_t1 = 0:pi/Res:h*2*pi-pi/Res;         %%%%%% ω*t1
Thita = L*omega_rf/v0 ;                    %%%%%%   θ0
X = 0.5*alfa*Thita;
omega_t2 = omega_t1 + Thita - X * sin(omega_t1);     %%%%%%   Eq.(8a)
%%%%%%%%%%%plot the Eq.(8a)%%%%%%%%%%%%%%%%%
for i= 1: h*Res*2;
x(i,:) = [omega_t1(i),omega_t2(i)];
y(i,:) = [0,L];
p = plot(x(i,:),y(i,:),'k');
hold on;
end
%%%%%%Schematic diagram of sine wave as modulating function%%%%%%%
x1 = 0:pi/1000:h*2*pi;
y1 = 0.025*sin(x1);
p = scatter(x1,y1,'.','b');
hold off;
%%%%%%%%%%%%%%%%%%%%%%%%%%%%%%%%%%%%%%%%%%%%%%%%%%%%%
```

2.MATLAB code for plotting Applegate diagram in Fig. 3

```
fclose all;
clear;
omega_rf = 2 * pi * 2856000000;            %%%%%MHZ
DCbeam_voltage = 350000;                   %%%%%kV
v0 = 239141636.9;                          %%%%%%m/s
L = 0.5;                                   %%%%%%meter
h = 2.5;                                   %%%%%%number of period
Res = 4;                                   %%%%%%%%%sample number
omega_t1 = 0:pi/Res:h*2*pi-pi/Res;         %%%%%% ω*t1
Thita = L*omega_rf/v0;                     %%%%%%θ0
omega_t2 = omega_t1 + Thita -pi*sawtooth(omega_t1-pi); %%%%%%   Eq.(18)
%%%%%%%%%%%plot the Eq.(18)%%%%%%%%%
for i= 1: h*Res*2;
x(i,:) = [omega_t1(i),omega_t2(i)];
y(i,:) = [0,L];
p = plot(x(i,:),y(i,:),'k');
hold on;
end
%%%%%Schematic diagram of sawtooth wave as modulating function%%%%%%%
x1 = 0:pi/2000:h*2*pi-pi/2000;
y1 = 0.025*sawtooth(x1-pi);
p = scatter(x1,y1,'.','b');
hold off;
%%%%%%%%%%%%%%%%%%%%%%%%%%%%%%%%%%%%%%%%%%%%%%%%%%%%%
```

3.MATLAB code for plotting right part of Applegate diagram in Fig. 4

```
fclose all;
clear;
omega_rf = 2 * pi * 2856000000;            %%%%%%MHZ
DCbeam_voltage = 350000;                   %%%%%kV
v0 = 239141636.9;                          %%%%%%m/s
L = 0.35;                                  %%%%%%meter
alfa = 0.15;                               %%%%%% alfa = V_1/V_0
h = 4;                                     %%%%%% number of period for ω*t1
Res = 4;                                   %%%%%%%%%sample number
omega_t1 = 0:pi/Res:h*2*pi-pi/Res;         %%%%%% ω*t1
Thita = L*omega_rf/v0 ;                    %%%%%%   θ0
omega_t2 = omega_t1 + Thita - 2 * sin(omega_t1) + sin(2*omega_t1) - 2*sin(3*omega_t1)/3;
%%% Eq. (20) with n=1,2,3
%%%%%%%%%%%plot the Eq. (20) with n=1,2,3%%%%%%%%
for i= 1: h*Res*2;
x(i,:) = [omega_t1(i),omega_t2(i)];
y(i,:) = [0,L];
p = plot(x(i,:),y(i,:),'k');
hold on;
end
%%%%%%Schematic diagram of sine wave as modulating function%%%%%%%
x1 = 0:pi/1000:h*2*pi;
y1 = 0.025*sin(x1);
y2 = -0.5*0.025*sin(2*x1);
y3 = 0.3333*0.025*sin(3*x1);
p = scatter(x1,y1,'.','b');
p = scatter(x1,y2,'.');
p = scatter(x1,y3,'.');
hold off;
%%%%%%%%%%%%%%%%%%%%%%%%%%%%%%%%%%%%%%%%%%%%%%%%%%%%%
```

4.MATLAB code for plotting Applegate diagram in Fig. 5

```
fclose all;
clear;
omega_rf = 2 * pi * 2856000000;            %%%%%MHZ
DCbeam_voltage = 350000;                   %%%%%kV
v0 = 239141636.9;                          %%%%%%m/s
L = 0.40                                   %%%%%%meter
l = [L/100: L/100: L]';                    %%%%%%
alfa = 0.13 ;                              %%%%%% alfa = V_1/V_0
P_f = 1.334E+09;                           %%%%%%%Reduced plasma_frequency
p_p_c = 5.579   ;                          %% Reduced plasma_propagation_constant
h = 2;                                     %%%%%% number of period for ω*t1
Res = 4;                                   %%%%%%%%%sample number
omega_t1 = 0:pi/Res:h*2*pi-pi/Res;         %%%%%% ω*t1
Thita = l*omega_rf/v0                      %%%%%%   θ0
X = 0.5*alfa*Thita;
SPC = sin(p_p_c.*l);
SPC1 = SPC./(p_p_c.*l);                    %%%%%% space charge factor
omega_t2 = omega_t1 + Thita - X .* SPC1 .* sin(omega_t1);     %%%%%%   Eq.(25)
%%%%%%%%%%%plot the Eq.(25)%%%%%%%%%
x = omega_t2;
for i= 1: h*Res*2;
y(:,i) = l;
p = plot(x(:,i),y(:,i),'k');
hold on;
end
%%%%%%Schematic diagram of sine wave as modulating function%%%%%%%
x1 = 0:pi/1000:h*2*pi-pi/1000;
y1 = 0.025*sin(x1);
p = scatter(x1,y1,'.','b');
hold off;
%%%%%%%%%%%%%%%%%%%%%%%%%%%%%%%%%%%%%%%%%%%%%%%%%%%%%
```